Structural Engineering and Mechanics, Vol. 33, No. 2 (2009) 215-238
DOI: http://dx.doi.org/10.12989/sem.2009.33.2.215

An improved pushover analysis procedure for multi-mode seismic performance evaluation of bridges : (1) Introduction to numerical model

Kwak, Hyo Gyoung† and Shin, Dong Kyu‡

Department of Civil and Environmental Engineering, Korea Advanced Institute of Science and Technology, 373-1 Guseong-dong, Yuseong-gu, Daejeon 305-701, Korea

(Received January 29, 2009, Accepted August 13, 2009)

Abstract. This paper introduces an improved modal pushover analysis (IMPA) which can effectively evaluate the seismic response of multi-span continuous bridge structures on the basis of modal pushover analysis (MPA). Differently from previous modal pushover analyses which cause the numerical unstability because of the occurrence of reversed relation between the pushover load and displacement, the proposed method eliminates this numerical instability and, in advance the coupling effects induced from the direct application of modal decomposition by introducing an identical stiffness ratio for each dynamic mode at the post-yielding stage together with an approximate elastic deformation. In addition to these two introductions, the use of an effective seismic load, calculated from the modal spatial force and applied as the distributed load, makes it possible to predict the dynamic responses of all bridge structures through a simpler analysis procedure than those in conventional modal pushover analyses. Finally, in order to establish validity and applicability of the proposed method, correlation studies between a rigorous nonlinear time history analysis and the proposed method were conducted for multi-span continuous bridges.

Keywords: bridges; improved modal pushover; identical stiffness ratio; equivalent modal load; elastic deformed shape.

1. Introduction

When structures are under strong ground motions, nonlinear behavior and large plastic deformation occurs. To estimate systems' ultimate enduring loading it is necessary to evaluate the exact systems' behavior under such cases. As a part of these efforts, a capacity-based design in the seismic design code has been adopted. The ATC-40 and FEMA-273 documents contain simplified nonlinear analysis procedures to determine the displacement demand imposed on a building expected to deform nonlinearly. However, ATC-40 follows an iterative method requiring analysis of a sequence of equivalent linear systems to avoid a dynamic analysis of the inelastic system. This approximate procedure produces substandard results (Chopra and Goel 1999). To improve the accuracy of results, a capacity-spectrum method that uses the well-known constant-ductility design

† Professor, Corresponding author, E-mail: khg@kaist.ac.kr
‡ Doctoral Course Student, E-mail: dongkyu.shin@gmail.com

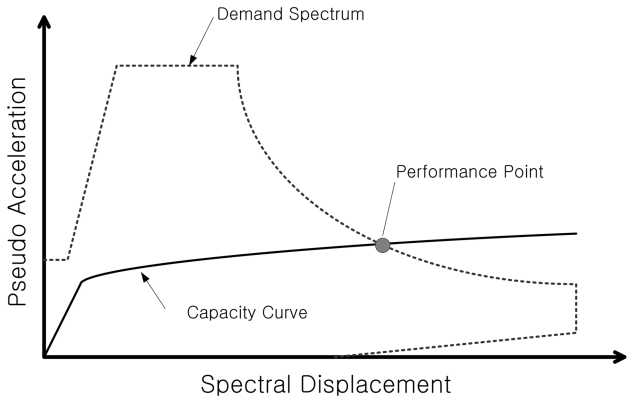

Fig. 1 Capacity spectrum method

spectrum for the demand diagram commonly referred to as the capacity spectrum method was developed by Freeman (1998). It conducts a seismic design and assessment on the basis of the application of an inelastic analysis. As shown in Fig. 1, by plotting the ensuing force-displacement curve obtained from an inelastic analysis of an idealized structural system, with appropriate transformations for dimensional consistency, onto a plot representing both the spectral displacement and accelerations of a composite spectrum, an acceptable deformation limit of structure is determined and defined as the performance point. The composite spectra represent the demand, whilst the capacity curve determined from the inelastic push-over analysis of a structure represents the supply (Elnashai 2001). Accordingly, the seismic design of a structure is conducted to reserve sufficient ductility while satisfying the demand.

The capacity spectrum method is appealing because it gives a visual representation of the supply-demand equation and allows simplicity in application. It requires the calculation of the capacity curve of the total structural system, expressed by a representative capacity curve in multi-degree degree-of-freedom (MDOF) structures. Among the many numerical methods for determining a capacity curve, three representative pushover analyses using the equivalent single-degree-of-freedom (ESDOF) system (Song 2004), the predominant single-degree-of-freedom (PSDOF) system (Usanmi *et al.* 2004) and a system in which all degrees of freedom (Chopra and Goel 2002) are popularly used.

First, a numerical method using ESDOF calculates the seismic response of a total structure using a representative vibration mode obtained from the force-displacement relationship, determined through the inelastic finite displacement analysis of a total structure subject to a uniformly distributed lateral load, as shown in Fig. 2(a). For bridges with a symmetric distribution of pier stiffness or with stiffer decks relative to piers, the fundamental mode dominates the structural response, allowing this method to be used reliably. For bridges in which this is not the case, however, the higher modal effects might be significant, and the accuracy of the pushover analysis may not be satisfactory (Zheng *et al.* 2003). On the other hand, a numerical method using PSDOF is based on the most dominant mode distribution. As all of the analysis procedures from the application of a lateral load (see Fig. 2(b)) to the pushover analysis are conducted with the most dominant vibration mode, the same limitations associated with the ESDOF method cannot be avoided (Krawinkler and Seneviratna 1998). This indicates that these limitations are induced essentially by ignoring other vibration modes.

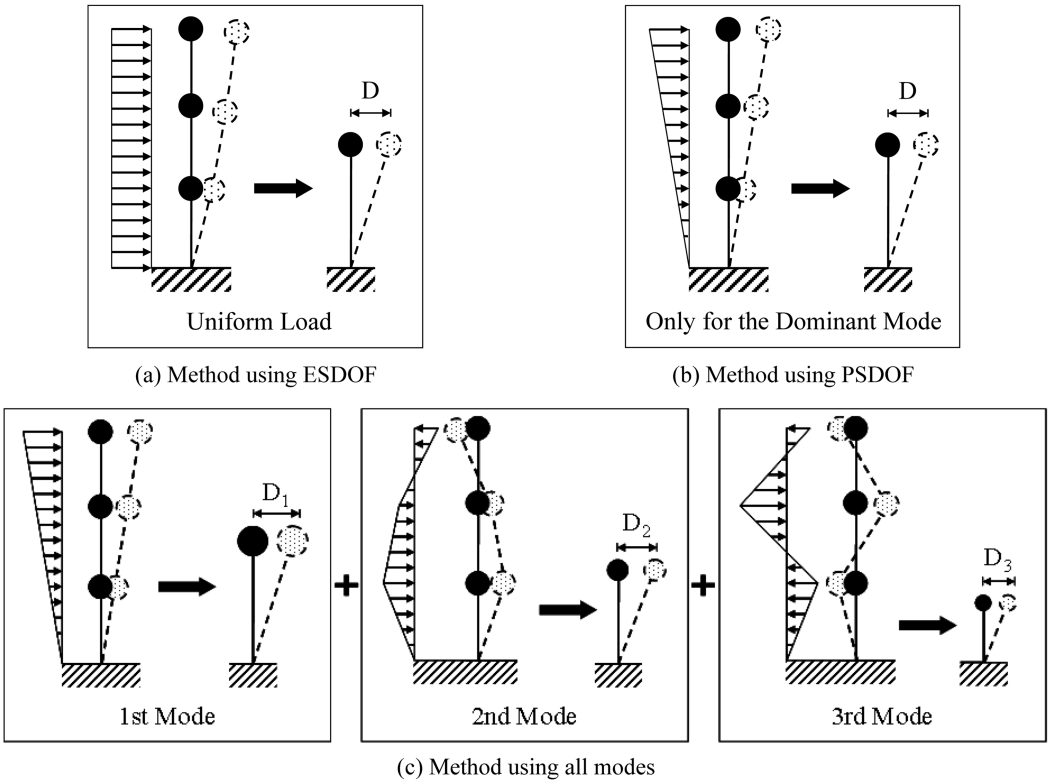

Fig. 2 Pushover analyses to determine the capacity curve of a multi-degree of freedom structure

Attempts were also made to consider more than a particular vibration mode in a pushover analysis in order to overcome these limitations, and the modal pushover analysis (MPA) based on structural dynamic theory was introduced (Chopra and Goel 2004). When using this method, as shown in Fig. 2(c), the modal capacity curves of a structure are determined by pushover analyses using the inertia force distribution for each mode. Combining all the modal seismic responses provides a reasonable estimate of the overall seismic behavior of the structure. This method can be used effectively in building structures (Chopra and Goel 2002) but it involves two characteristic drawbacks in a direct application to multi-span continuous bridges. First, unlike building structures that have typical vibration modes regardless of the number of floors, bridge structures represent remarkably different capacity curves at every pier, corresponding to each vibration mode due to the change in the stiffness ratio between the bridge deck and pier (See Fig. 3(a)). This causes the analysis procedure to become exceedingly complex. Second, the capacity curve, which does not show the monotonically increasing feature (as is shown in the elastic behavior) may appear (See Fig. 3(b)). This makes it impossible to apply the modal pushover analysis to bridge structures because the negative work cannot be defined in a structural system.

Accordingly, this paper introduces an improved modal pushover analysis (IMPA) that can be used effectively even in the analysis of multi-span continuous bridges. As only one pushover curve for each vibration mode is required and the numerical instability when determining the pushover curve is removed, all of the procedures related to the determination of capacity curves as well as those related to the modal superposition are simplified while maintaining the advantages of the modal

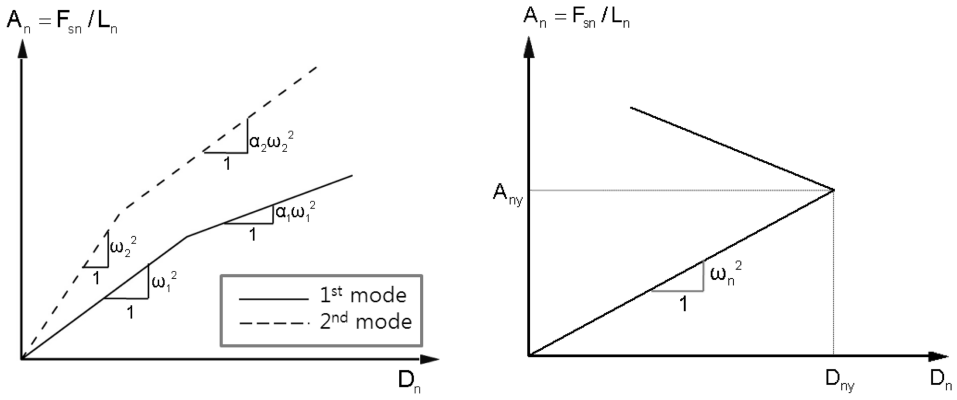

(a) Differences in the post-yield stiffness ratio (b) Negative work in the SDOF pushover curve

Fig. 3 Pushover curves in MPA represented in A-D format

pushover analysis. The validity of the introduced model is established by comparing the obtained numerical results of four example bridges with those obtained using a nonlinear time history analysis. Correlation studies with the modal pushover analysis show the efficiency of the proposed model.

2. Modal pushover analysis (MPA)

Based on the modal analysis to determine the dynamic response of multi-degree-of-freedom systems, the modal pushover analysis (MPA) was introduced by Chopra and Goel (2002) and was applied to multi-story building structures. In addition, many seismic design codes such as ATC-40 and FEMA-274 have adopted this method due to its simplicity in application. The peak response of a structure due to each vibration mode of the structure can be determined by a pushover analysis when it is subjected to lateral modal forces distributed over the height of the building according to its corresponding vibration mode.

A general dynamic equilibrium equation for a N^{th}-degree-of-freedom system subjected to ground acceleration $\ddot{u}_g(t)$ can be expressed as

$$[\mathbf{m}]\{\ddot{\mathbf{u}}\} + [\mathbf{c}]\{\dot{\mathbf{u}}\} + \{\mathbf{f}_s(\mathbf{u}, \dot{\mathbf{u}})\} = -[\mathbf{m}]\{\mathbf{1}\}\ddot{u}_g(t) = \{P_{eff}(t)\} \tag{1}$$

where $\{\mathbf{u}\}$ is the relative displacement to the ground, $[\mathbf{m}]$ and $[\mathbf{c}]$ are respectively the mass and damping matrixes of the system, $\{\mathbf{f}_s\}$ is the resisting force, and $\{\mathbf{1}\}$ is a vector of order N with each element equal to unity (Chopra 2001). Additionally, the spatial distribution of the effective earthquake force $\{P_{eff}(t)\}$ defined on the right side in Eq. (1) can be interpreted as the sum of the modal spatial force vector $\{\mathbf{s}_n\}$ with the elastic mode shape $\{\phi_n\}$.

$$\{\mathbf{p}_{eff}(t)\} = \sum_{n=1}^{N} \{\mathbf{p}_{eff,n}(t)\} = \sum_{n=1}^{N} -\{\mathbf{s}_n\}\ddot{u}_g(t) = \sum_{n=1}^{N} -\Gamma_n[\mathbf{m}]\{\boldsymbol{\phi}_n\}\ddot{u}_g(t) \tag{2}$$

Here, Γ_n is a modal participation factor based on the linear-elastic mode shape $\{\phi_n\}^T$ normalized with respect to the modal pushover roof displacement u_{rn}.

As any set of N independent vectors can be used as a basis for representing any other vector of order N, the lateral displacement vector $\{u\}$ can be expanded

$$\{u\} = \sum_{n=1}^{N} \{u_n\} = \sum_{n=1}^{N} \{\phi_n\} q_n \tag{3}$$

Here, q_n represents the modal amplitude.

Finally, substituting Eq. (3) and its derivatives into Eq. (1), pre-multiplying by $\{\phi_n\}^T$, and using the mass and damping orthogonality of the mode shapes results in the following governing equation for a SDOF system

$$\ddot{D}_n + 2\zeta_n \omega_n \dot{D}_n + \frac{F_{sn}}{L_n} = -\ddot{u}_g(t),\ F_{sn}(D_n, \dot{D}_n) = \{\boldsymbol{\phi}_n\}^T \{\mathbf{f}_s(D_n, \dot{D}_n)\} \tag{4}$$

In Eq. (4), $F_{sn} = \{\phi_n\}^T \{f_n(D_n, \dot{D}_n)\}$ is the modal internal resisting force, D_n is the modal displacement (with $\dot{D}_n$ and $\ddot{D}_n$ representing the modal velocity and acceleration, respectively), L_n is $\{\phi_n\}^T [m]\{1\}$ and ζ_n and ω_n are the modal damping and frequency, respectively.

Eq. (4) can be solved either by conducting a nonlinear SDOF dynamic time-history analysis or by using the nonlinear SDOF displacement response spectrum. In order to solve Eq. (4), equivalent nonlinear SDOF representations of the structure must be defined for the relationship between F_{sn} and D_n. This relationship should be determined by a displacement-controlled nonlinear static analysis of the structure as the structure undergoes displacement $\{u\} = \phi_n q_n = \Gamma_n \phi_n D_n$ as D_n increases. However, this type of analysis is not supported by commercially available software. Therefore, in the modal pushover analysis, a force-controlled pushover analysis is initially conducted in order to determine the relationship between the base shear and the roof displacement with force distribution $\{s_n\}$, which is the only lateral force distribution that can produce displacements proportional to $\{\phi_n\}$ according to uncoupled modal response history analysis theory. This relationship obtained from the pushover analysis of the structure is then converted into an equivalent SDOF pseudo-acceleration A_n versus displacement relationship D_n using the following equation

$$A_n = \frac{V_{bn}}{M_n^*} = \frac{V_{bn}}{\Gamma_n L_n} = \frac{F_{sn}}{L_n},\ D_n = \frac{u_{rn}}{\Gamma_n \phi_{rn}} \tag{5}$$

In this equation, $M_n^* = \Gamma_n L_n$ represents the effective modal mass. Additional details and assumptions related to the above formulation can be found in the literature (Chopra and Goel 2002).

Although this method gives good estimations for the entire seismic response of building structures, several limitations exist in a direct application to bridge structures related to the following disadvantages: (1) according to classical modal analysis theory (Nickell 1976), it is impossible to superpose modal responses of nonlinear structures due not only to the coupling phenomenon that exists between the governing differential equations for the N modes but also as a result of the changes in the vibration properties of the structure. In other words, the use of $\{s_n\}$ as the modal lateral force distribution vector is not based on nonlinear theory (i.e., is not unique); (2) in order to define the relationship between F_{sn} and D_n in each vibration mode, the modal pushover analysis procedure requires as many static pushover analyses of the structure as the number of modes considered; (3) as a possible limitation of the modal pushover analysis procedure, reversal in the pushover load versus displacement relationships of the structure under higher-mode lateral force distributions is possible, resulting in an unstable solution (see Fig. 3(b)); and (4), finally, if nonlinear

SDOF displacement response spectra (in place of dynamic time-history analyses) are used to solve Eq. (4), the use of different response spectrum may be needed for each mode, as nonlinear response spectra depend on the post-yield stiffness ratio of the structure, which would be different for each vibration mode.

3. Improved modal pushover analysis (IMPA)

If it is possible to assume that a time-dependent coefficient $\alpha(t)$ exists that satisfies the relationship between the time variant stiffness $[k(t)]$ and the initial elastic stiffness matrix $[k_0]$ as $[\boldsymbol{k}(t)] = \alpha(t)[\boldsymbol{k}_0]$ and, in addition, that satisfies the relationship between a time variant natural frequency $\omega(t)$ and initial elastic natural frequency ω_0 as $\omega(t)^2 = \alpha(t)\omega_0^2$ regardless of the modes, the mode shape $\{\phi_0\}$ defined in the elastic region would not vary after yielding, as shown in Eq. (6), and implying that the mutual coupling effect among the vibration modes would not occur, as non-diagonal terms in the governing equation of motion multiplied by $\{\phi_0\}^T$ become zero. Therefore, the introduction of this assumption makes it possible to divide the governing equation of motion for a N^{th}-degree-of-freedom system into independent N governing equations defined at each vibration mode. This uncoupled characteristic remains even after the structure yields (see Eq. (4)). Here, as shown in Fig. 4, $\alpha(t)$ denotes the post-yield stiffness ratio in the modal pushover curve defined in the A-D domain.

$$([\mathbf{k}(t)]-\omega^2[\mathbf{m}])\{\phi\} = \alpha(t)([\mathbf{k}_0]-\omega_0^2[\mathbf{m}])\{\phi_0\} = 0, \therefore\{\phi\},\{\phi_0\} \tag{6}$$

Here, an additional assumption needs to be introduced. If a pushover analysis for bridge structures is conducted on the basis of classical elastic theory, the deformation shape developed by the application of a lateral load would not change and would instead become enlarged in proportion to the magnitude of the applied load. In effect, in this case, the deformation shape changes and shows a different configuration compared to that obtained in the elastic stage as any one of piers starts to yield. Nevertheless, to maintain the assumed relationship of $[\boldsymbol{k}(t)] = \alpha(t)[\boldsymbol{k}_0]$ even after the yielding of a pier, the deformation shape obtained after the structure yields must be adjusted to the approximated

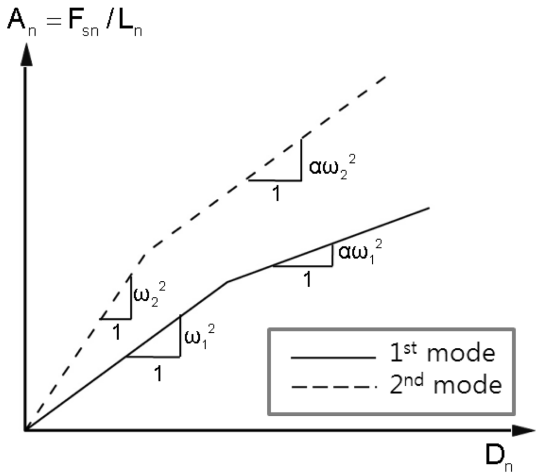

Fig. 4 Pushover curves defined in A-D format in IMPA

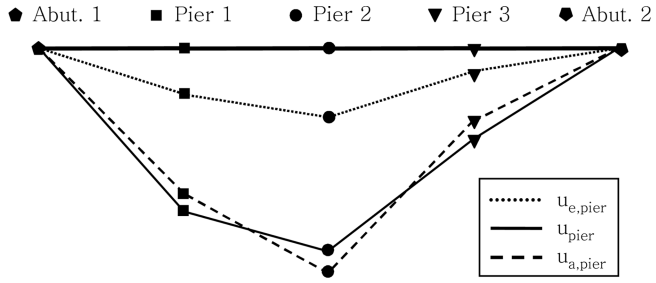

Fig. 5 The inelastic and approximated displacement of a four-span bridge

elastic deformation that maintains the elastic deformation shape. Fig. 5 shows an example that defines the approximated elastic deformation for a four-span continuous bridge structure with equal span lengths.

In Fig. 5, $u_{e,pier}$ describes an upper-bound elastic deformation shape at which one of the piers just starts to yield (pier 2 in this example bridge), and u_{pier} describes the inelastic deformation obtained when the entire structure reaches the fully plastic stage. Therefore, the approximated elastic deformation of the r^{th} pier $u_{a,pier_r}$ can be defined as

$$u_{a,pier_r} = \beta u_{e,pier_r} \tag{7}$$

Here, $u_{e,pier_r}$ denotes the upper-bound elastic deformation shape of the r^{th} pier and is a coefficient that satisfies $\beta = \text{Min}\left(\sum_{r=1}^{m}(u_{pier_r} - \beta u_{e,pier_r})^2\right)$ in which m represents the number of piers. Finally, the use of $\alpha(t)$ and $u_{a,pier}$ calculated by Eq. (7) instead of u_{pier} at the yielding stage makes it possible to maintain the basic assumptions adopted in the MPA effectively, even at the yielding stage. This leads to a simpler analytical procedure compared to that conducted in the conventional MAP, as the stiffness ratio $\alpha(t)$ at each pier has the same value and maintains consistency regardless of the change in the vibration modes.

As mentioned previously, a direct application of the conventional MPA to multiple continuous bridges requires multiple pushover analyses in order to allow for the effects by higher vibration modes and may represent the displacement reversal (described as the negative work in Fig. 3(b)), which makes it impossible to continue the structural analysis at the yielding stage. Therefore, this paper introduces a solution procedure to remove all of these defects. First, an equivalent load distribution that can develop a monotonically increasing capacity curve at all piers without any displacement reversal is proposed.

Given that the applied seismic load $\{P_{eff}\}$ in Eq. (1) is proportional to $[m]\{1\} = \sum_{n=1}^{N}\{S_n\} = \sum_{n=1}^{N}\Gamma_n[m]\{\phi_n\}$ (see Eq. (2)), the effective seismic load $\{P\}$ applied to the structure for the pushover analysis can be defined as a linear combination of each modal force effect: $\{P\} = \gamma\sum_{n=1}^{N} a_n\Gamma_n[m]\{\phi_n\}$, where γ is the proportional loading factor and α_n is a weighting factor reflecting the contribution of each modal effect. In addition, the pushover analysis is based on the static analysis, implying that the acceleration and damping components $\ddot{D}_n$ and $\dot{D}_n$, respectively, become zero in Eq. (4). Thus, the remaining components in the governing equation can be rewritten as

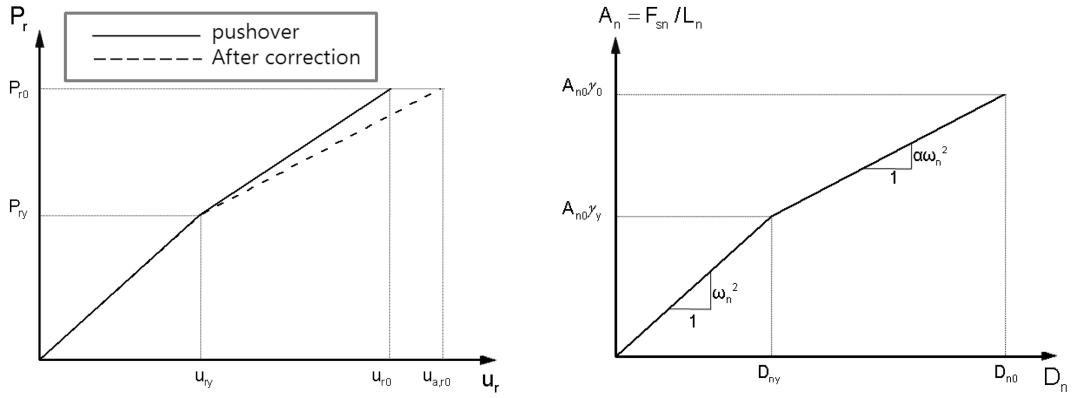

(a) Inelastic load-displacement relationship (b) A-D relationship

Fig. 6 Converting the inelastic load-displacement relationship to an A-D relationship

$$\omega_n^2 D_n = \frac{\{\phi_n\}^T\{\mathbf{P}\}}{\Gamma_n M_n} = \frac{\{\phi_n\}^T \gamma \sum_{i=1}^{N}(a_i \times \Gamma_i[\mathbf{m}]\{\phi_i\})}{\Gamma_n M_n} = \gamma \times a_n \tag{8}$$

If the pseudo acceleration at the elastic stage is defined as A_{no}, the relationship of $\omega_n^2 D = \gamma a_n = A_{n0}$ can be obtained. This relationship assumed to be approximately satisfied up to the yielding stage. The uniformly distributed effective seismic load $\{P\}$ can then be expressed by

$$\{\mathbf{P}\} = \gamma \sum_{i=1}^{N}(A_{i0}\Gamma_i[\mathbf{m}]\{\phi_i\}) \tag{9}$$

The sequential application of this load $\{P\}$ with a monotonic increase of the proportional loading factor produces an inelastic force-displacement relationship, as shown in the results of the pushover analysis (see the continuous line in Fig. 6(a)). Correlation of this relationship with Eq. (7) (see the dotted line in Fig. 6(a)) and conversion to an A-D relationship then follow, in which the corresponding pseudo acceleration A_n in Fig. 6(b) is represented by $A_n = A_{no}\gamma$. In particular, as shown in Fig. 6(b), the slope of the relationship between A_n and D_n in the elastic stage represents ω_n^2, the modal displacements D_{ny} corresponding to the initial yielding of structure. D_0, which corresponds to the ultimate loading, can be determined by

$$D_{ny} = \frac{\gamma_y A_{n0}}{\omega_n^2}, \quad D_{n0} = D_{ny} + \frac{A_{n0}(\gamma_0 - \gamma_y)}{\alpha\omega_n^2} \tag{10}$$

Here, γ_y and γ_0 denote the proportional loading factors determined at the beginning of the structural yielding and failure processes, respectively.

Additionally, the post-yielding stiffness ratio α must be determined to define the unique relationship between A_n and D_n, as was assumed in IMPA. Using the relationships in Eq. (10), the displacements of the r^{th} pier, u_{ry}^* and $u_{a,r0}^*$ corresponding to the initial yielding and ultimate loading stage, respectively, can be calculated by superposing all of the modal yield and ultimate displacements.

$$u_{ry}^* = \sum_{n=1}^{N} u_{rny} = \sum_{n=1}^{N}(\phi_{rn}\Gamma_n D_{ny}) = \sum_{n=1}^{N}\left(\frac{\phi_{rn}\Gamma_n A_{n0}\gamma_y}{\omega_n^2}\right)$$

$$u_{a,r0}^{*} = \sum_{n=1}^{N} u_{rn0} = \sum_{n=1}^{N} \left\{ \phi_{rn} \Gamma_n \left(\frac{A_{n0}\gamma_y}{\omega_n^2} + \frac{A_{n0}(\gamma_0 - \gamma_y)}{\alpha \omega_n^2} \right) \right\} \tag{11}$$

The displacements u_{ry}^{*} and $u_{a,r0}^{*}$ calculated by Eq. (11) must then be identical to the corrected displacements u_{ry} and $u_{a,ro}$, respectively, in Fig. 6(a). This determines the load-displacement relationship obtained from the pushover analysis. Therefore, the equality of both components ($u_{ry} = u_{ry}^{*}$ and $u_{a,ro} = u_{a,r0}^{*}$) leads to the following relationship of the constant post-yielding stiffness ratio (see Eq. (12)). This equation also shows that the ratio α can be obtained directly from the inelastic pushover curve.

$$\alpha = \frac{\gamma_0 - \gamma_y}{u_{a,r0} - u_{ry}} \times \frac{u_{ry}}{\gamma_y} \tag{12}$$

The solution procedure for the introduced IMPA is described here as a sequence of steps:

(1) Conduct sequential pushover analyses with an increase of the proposed load distribution in Eq. (9) up to the collapse of structure.
(2) Determine the proportional loading factors γ corresponding to the structural yielding and collapse.
(3) Adjust the finally obtained inelastic deformation u_{pier} to an approximated elastic deformation $u_{a,pier}$ (see Fig. 5) according to the criterion in Eq. (7).
(4) Determine the modal pushover curve from the result of Steps (2) and (3).
(5) Calculate the post-yielding stiffness ratio α using Eq. (12).
(6) Find the modal ultimate displacement D_{n0} by solving the time history in Eq. (4) or by using the capacity spectrum method for a SDOF system.
(7) Calculate the ultimate displacement of a MDOF system by superposing the modal displacements.

4. Numerical studies

4.1 Numerical examples and ground accelerations

In order to establish the validity and applicability of the proposed procedure in IMPA, correlation studies between a nonlinear time history analysis (Lakshmanan *et al.* 2009) and IMPA were conducted. To study the typical structural behavior according to the change in various influencing factors, such as the symmetry and the stiffness ratio of a super-structure to a pier, four four-span continuous RC bridge models were investigated. As shown in Fig. 8, B12 represents a symmetrical configuration of the sub-structures, while B22 and B32 are unsymmetrical arrangements of the lengths of the piers. In advance, B42 has a sub-structure that is identical to that of B32, except that the stiffness of the superstructure is assumed to be one-tenth that of B32. The connections between the super-structure and the pier and the weight density of the structure, $\gamma = 2.3$ ton/m^3, are assumed. In particular, as the nonlinear behavior of a bridge due to earthquake loading is concentrated on the pier, and exact evaluation of the resisting capacity of the piers is a prerequisite for the seismic analysis of the bridge; the resisting capacity of a pier is calculated on the basis of the assumption that a total of 198D29 reinforcing bars with a yielding stress of $f_y = 4000$ kg/cm^2 are uniformly embedded in a section. The sectional properties and configuration of each bridge are shown in

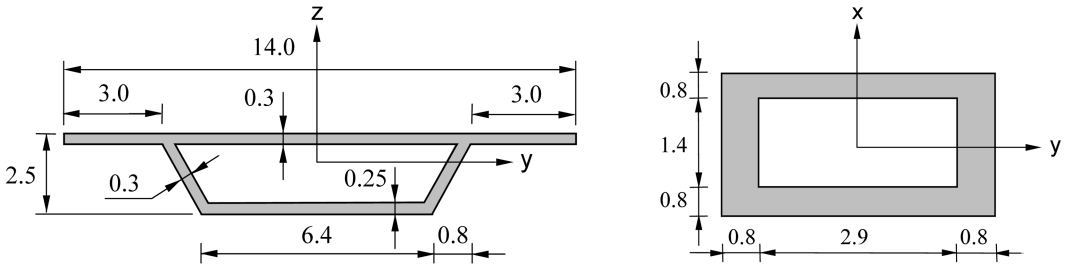

(a) super-structure (deck) (b) sub-structure (pier)

Fig. 7 Section details for example bridge (unit: m)

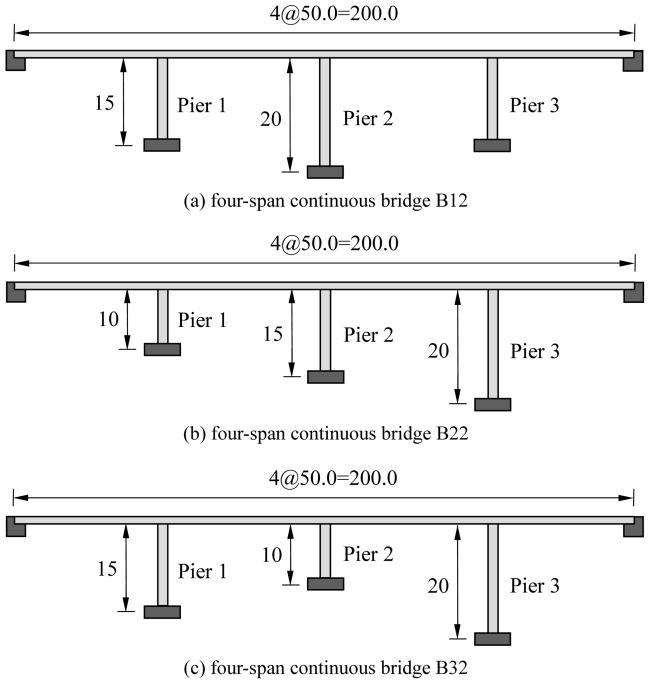

(a) four-span continuous bridge B12

(b) four-span continuous bridge B22

(c) four-span continuous bridge B32

Fig. 8 Geometry of example bridges (unit : m)

Figs. 7 and 8, respectively.

Generally, due to the relatively strong bending stiffness of a super-structure in the longitudinal direction, the longitudinal behavior of a multi-span bridge under earthquake loading is does not differ from the equivalent single-degree-of-freedom behavior, implying that the seismic behavior of bridge structures is dominantly affected by the structural response in the transverse direction. Therefore, this paper concentrates primarily on a comparison of structural responses in the transverse direction. Moreover, to simulate the nonlinearity in a pier effectively, as it is concentrically developed at the end region connected to the foundation, the plastic hinge length is taken into account. The obtained nonlinear moment-curvature relationships for each pier are then idealized as a bi-linear relationship; the corresponding material properties to an idealized moment-curvature envelope curve can then be determined, as shown in Table 1. 5% Rayleigh damping is used, and the hysteretic behavior according to the application of earthquake loading is evaluated on the basis of

Table 1 Material in an idealized moment-curvature relationship

Flexural Stiffness (EI)	Yielding curvature (ϕ_y)	Post yield stiffness ratio (α)
39805.6 MN-m	0.0036	0.0001

Table 2 Artificial ground accelerations

No.	EQ 1	EQ 2	EQ 3	EQ 4	EQ 5	EQ 6	EQ 7
Earthquake	California	El Centro	Mexico City	Northridge	San Fernando	San Francisco	Taft
Year	1933	1940	1985	1994	1971	1957	1952
Comp.	S07E	S00E	SCTS00E	CHAN3	N76W	S09E	EW

the bi-linear stiffness degrading model introduced by Takeda *et al.* (1970), as this model effectively simulates the structural responses of RC structures.

Linear and nonlinear analyses of the multi-span bridges were conducted using the Opensees program. To verify the effectiveness of the introduced method (IMPA), the structural responses according to the four different approximated methods of ESDOF, PSDOF, MPA and IMPA were calculated and compared with the reference response obtained from the nonlinear time history analysis. For these correlation studies, seven artificial ground accelerations were used, as shown in Table 2. They were developed by adjusting the maximum acceleration to 1.0G. These ground motion records were scaled to a peak ground acceleration of 1.0g; they are referred to as EQ1 to EQ7 alphabetically.

4.2 Comparison to established methods

Correlation studies between the proposed method IMPA and the established methods of ESDOF, PSDOF and MPA were conducted with the objective of establishing the applicability and validity of the proposed method. Bridges B32 and B42, which have the largest unsymmetrical configuration of piers among the example structures in Fig. 8, were selected, and a ground acceleration of EQ4 (Northridge) in Table 2 was adopted in the nonlinear analysis, as a reassessment of conventional seismic design procedures and careful consideration of uncertainties were undertaken after the great amount of structural damage caused by this earthquake (Bozorgnia and Bertero 2004).

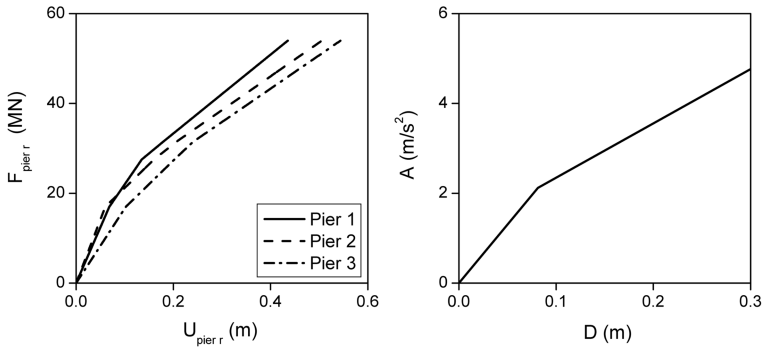

(a) $F-u$ relationship (b) A-D relationship

Fig. 9 Load-displacement and A-D relationships of B32 constructed by ESDOF

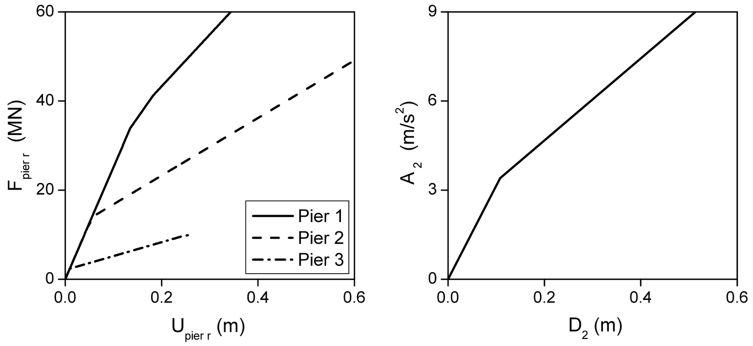

(a) $F-u$ relationship (b) A-D relationship

Fig. 10 Load-displacement and A-D relationships of B32 constructed by PSDOF

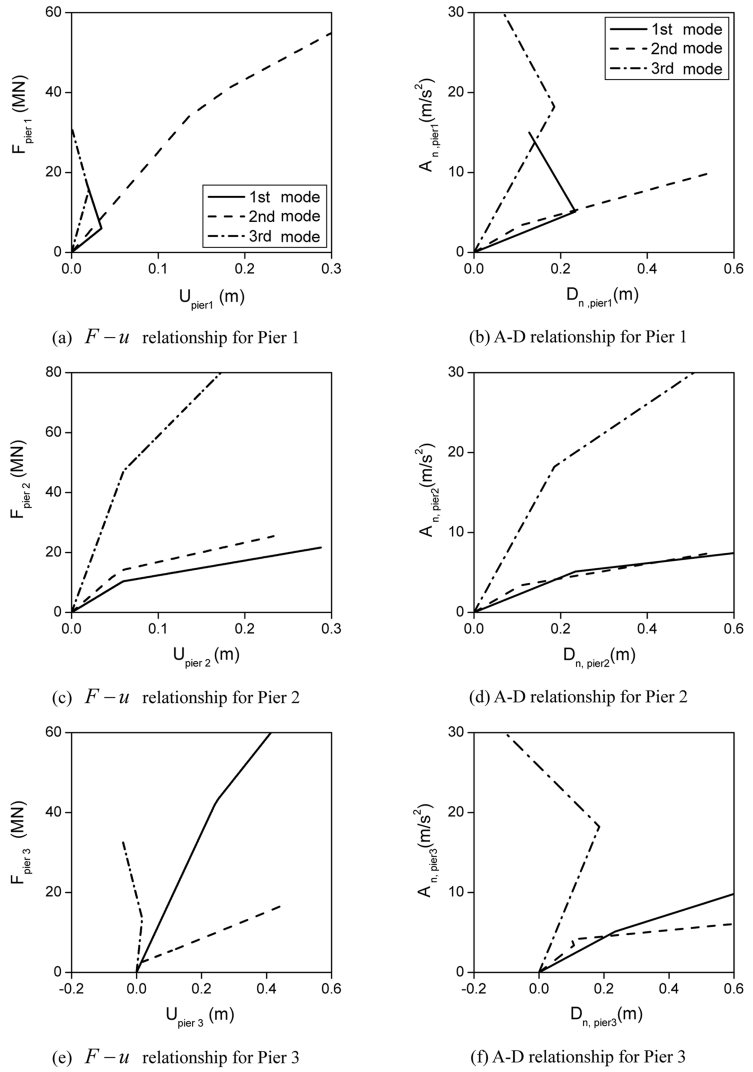

(a) $F-u$ relationship for Pier 1 (b) A-D relationship for Pier 1

(c) $F-u$ relationship for Pier 2 (d) A-D relationship for Pier 2

(e) $F-u$ relationship for Pier 3 (f) A-D relationship for Pier 3

Fig. 11 Load-displacement and A-D relationships of B32 constructed by MPA

As mentioned earlier, the relationship between $A_n = F_{sn}/L_n$ and D_n can be determined by converting the load-displacement relationship obtained by applying the load distribution defined at each method. Figs. 9 to 11 show the load-displacement relationship of $F-u$ and the corresponding relationship between $A_n = F_{sn}/L_n$ and D_n according to ESDOF, PSDOF and MPA, respectively. In the case of PSDOF, a load distribution s_2 was used to determine the load-displacement relationship, as the effective modal mass of the second mode is nearly 58.3% larger than those of the other modes. A comparison of ESDOF and PSDOF with MPA shows that MPA requires more complicated solution procedures for the seismic analysis of bridges because the capacity curves for each mode at each pier (nine different curves in B32 with three piers) must be determined due to the different post-yielding stiffness ratios of these curves. Furthermore, as a possible limitation in a direct application of MPA to multi-span continuous bridges, the load versus the displacement relationships of the structure may represent the displacement reversal, as shown in Figs. 11(b) and (f) under higher-mode lateral force distributions.

In contrast, the introduced method, IMPA, which requires only one pushover analysis with the proposed load distribution, produces an appropriate capacity curve representing a monotonically increasing feature without any displacement reversal, even in higher modes. Fig. 12 shows the load-displacement relationship for pier 1 and the converted corresponding $A-D$ relationship in B32. As mentioned above, IMPA produces identical A-D relationships to those in Fig. 12(b) with other piers, in spite of the different load-displacement relationship from that in Fig. 12(a), due to the application of the uniformly distributed effective seismic load $\{P\}$ in Eq. (9) and the introduction of the constant post-yielding stiffness ratio α in Eq. (12). As the converted $A-D$ relationships at the other piers will be identical to that of pier 1, it becomes possible to estimate the seismic responses of the other piers with the use of the capacity curve for pier 1.

Based on the converted $A-D$ relationships determined by the four different methods (including IMPA), nonlinear time history analyses were conducted using Opensees to compare the relative validity and accuracy of each method. In contrast to other methods, however, MPA does not allow a time history analysis to be conducted over the elastic range due to the displacement reversal in the converted $A-D$ relationship at the post-yielding stage (see circle in Figs. 15(a) and 15(c)). As shown in Fig. 13, the ESDOF result is in very good agreement with the result of the nonlinear time history analysis (NHA) for the unsymmetrical bridge B32. This is consistent with established research result that shows that ESDOF gives feasible predictions when the level of stiffness of the

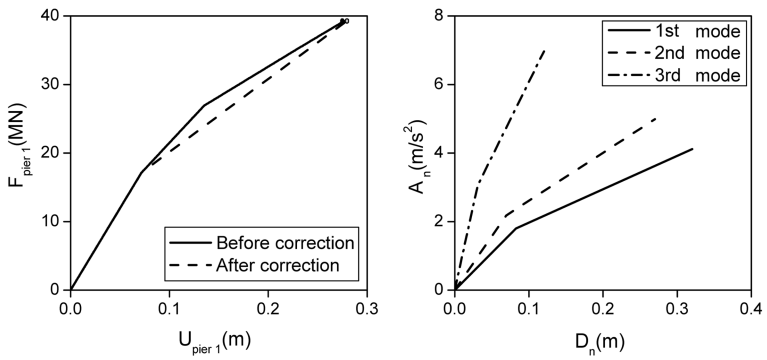

(a) $F-u$ relationship (b) A-D relationship

Fig. 12 Load-displacement and A-D relationships of B32 constructed by IMPA

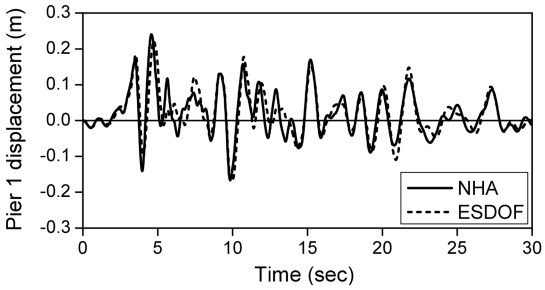

(a) Time history response of pier 1

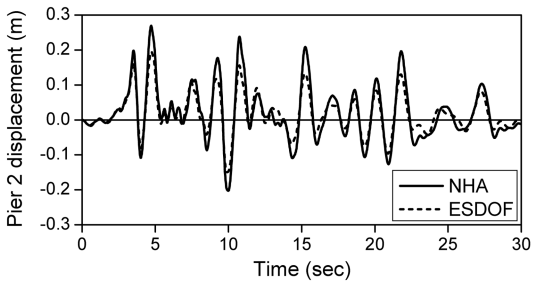

(b) Time history response of pier 2

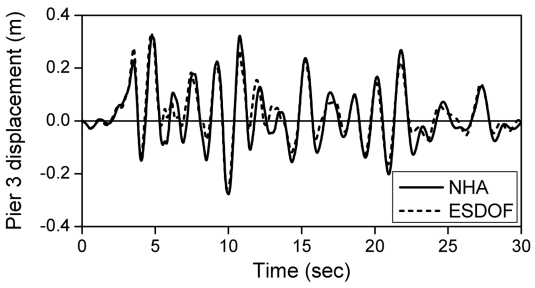

(c) Time history response of pier 3

Fig. 13 Time history response of B32 using ESDOF (Northridge EQ)

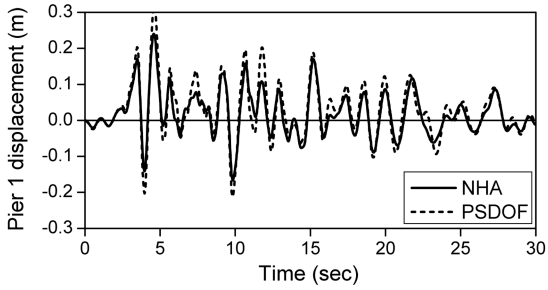

(a) Time history response of pier 1

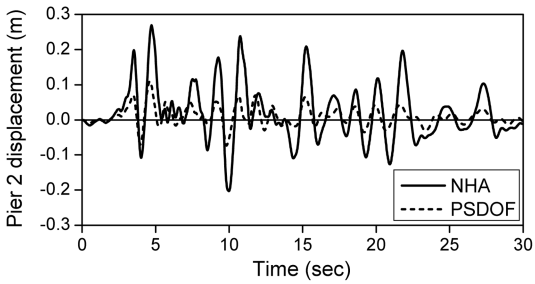

(b) Time history response of pier 2

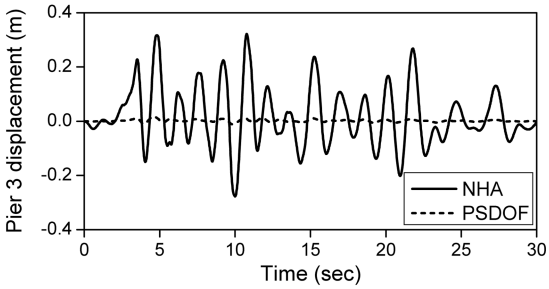

(c) Time history response of pier 3

Fig. 14 Time history response of B32 using PSDOF (Northridge EQ)

super-structure is relatively higher than that of the sub-structures (Usanmi *et al.* 2004). In contrast, PSDOF in Fig. 14, which considers only one representative mode, is not in good agreement with the nonlinear time history analysis result, especially in piers 2 and 3, as the other modes also have a strong effect on the response, as does the representative mode in the case of an unsymmetrical bridge such as bridge B32.

Fig. 15 shows the nonlinear time history response of B32 calculated by MPA. In spite of a more rigorous method compared to the previous two methods of ESDOF and PSDOF, the analysis by MPA is interrupted at piers 1 and 3 after approximately five seconds due to the displacement reversal in the converted $A-D$ relationship. These interrupted points are marked as circles in Figs. 15(a) and Fig. 15(c). Although the response of pier 2 can be estimated using the method of the

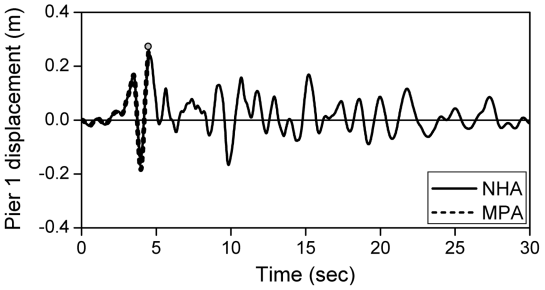

(a) Time history response of pier 1

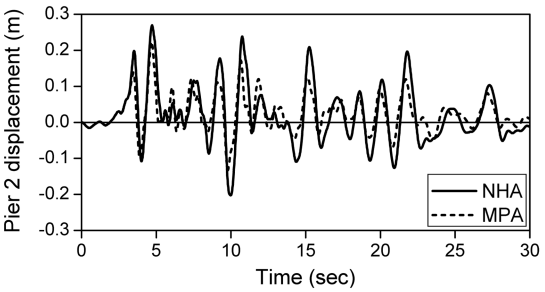

(b) Time history response of pier 2

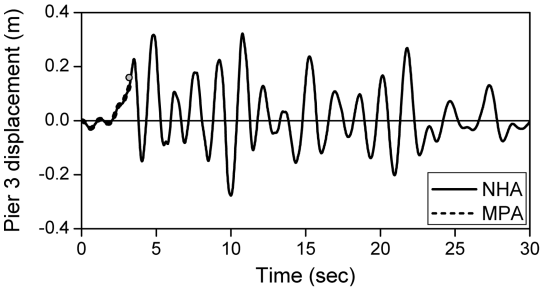

(c) Time history response of pier 3

Fig. 15 Time history response of B32 using MPA (Northridge EQ)

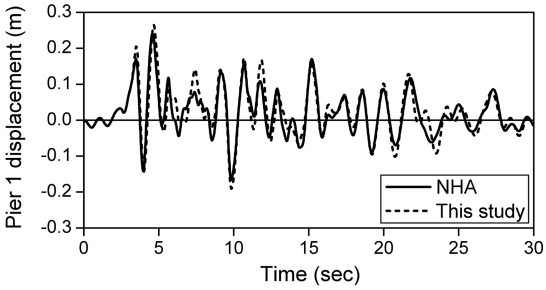

(a) Time history response of pier 1

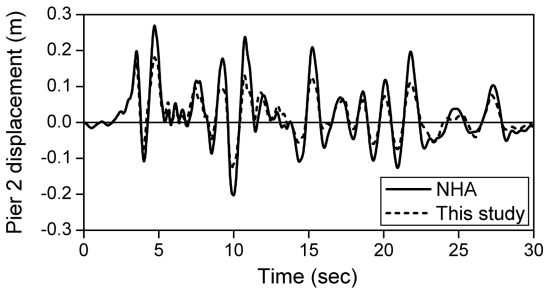

(b) Time history response of pier 2

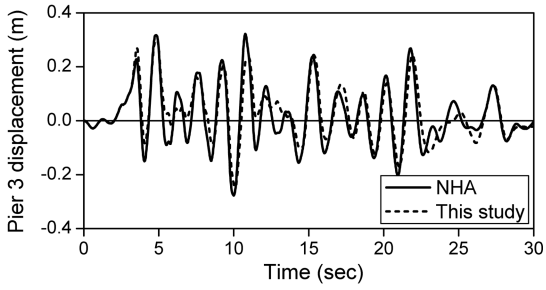

(c) Time history response of pier 3

Fig. 16 Time history response of B32 using IMPA (Northridge EQ)

nonlinear time history, a modification of the procedure is required for a robust analysis. Finally, a comparison was also made for the responses of bridge B32 as obtained using the proposed method and the nonlinear time history analysis (NHA). The result of this comparison is shown in Fig. 16. The results of the proposed method are in good agreement with the nonlinear time history analysis, apart from an insignificant error at pier 2. This result implies that the proposed method (IMPA) can be applied effectively to calculate the time history responses for unsymmetrical bridge structures when the stiffness of the superstructure is greater than that of the sub-structure.

To compare the effectiveness and validity of each method, an additional correlation study was conducted for bridge B42, in which the stiffness levels of the sub-structure piers are much greater than that of the super-structure. The nonlinear time history responses determined by each method

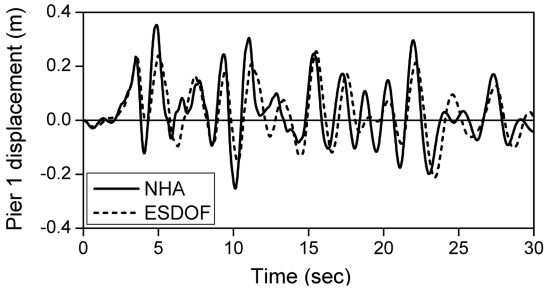

(a) Time history response of pier 1

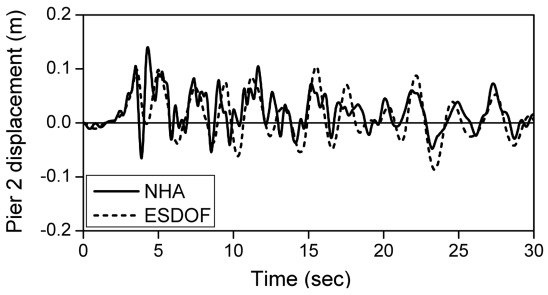

(b) Time history response of pier 2

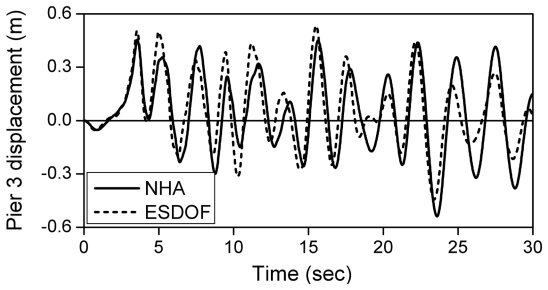

(c) Time history response of pier 3

Fig. 17 Time history response of B42 using ESDOF (Northridge EQ)

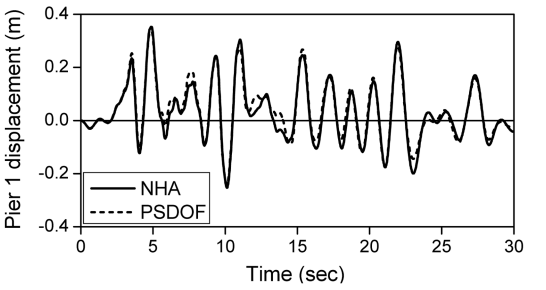

(a) Time history response of pier 1

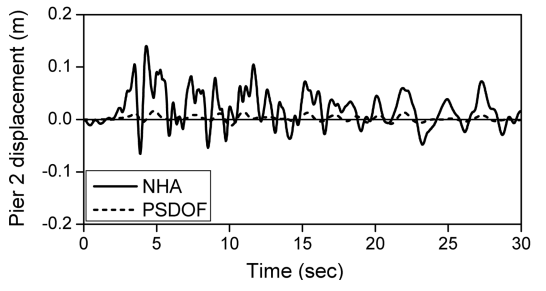

(b) Time history response of pier 2

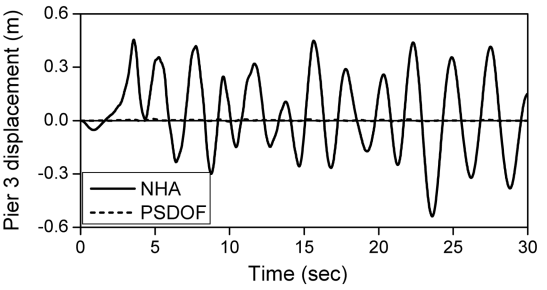

(c) Time history response of pier 3

Fig. 18 Time history response of B42 using PSDOF (Northridge EQ)

are shown in Figs. 17 to 20 together with the reference responses obtained from an exact time-history analysis (NHA) of the entire structure. As shown in these figures, PSDOF and MPA cannot estimate the nonlinear time history response for the unsymmetrical bridge B42. In particular, in spite of the fairly satisfactory agreement with the data of bridge B32, ESDOF cannot effectively simulate the nonlinear time history response of bridge B42 (see Fig. 17). On the other hand, as shown in Fig. 20, the proposed method is in good agreement with the nonlinear time history response of bridge B42. A careful investigation based on a comparison of the numerical results resulted in the following observations: (1) when ESDOF is applied to a bridge with a relatively weak super-structure stiffness, such as bridge B42, a successful estimation cannot be expected; (2) PSDOF can be applied only to a symmetrical bridge; (3) occasionally, the use of MPA is impossible when

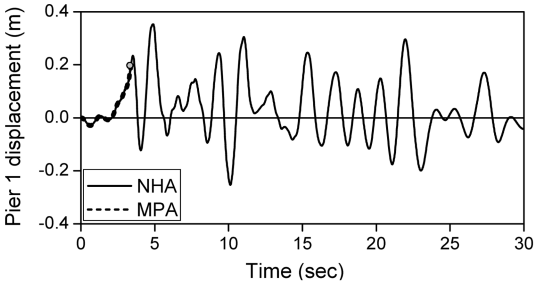

(a) Time history response of pier 1

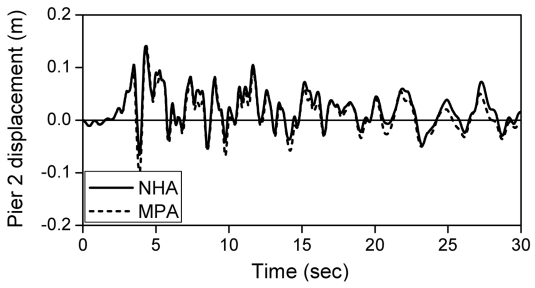

(b) Time history response of pier 2

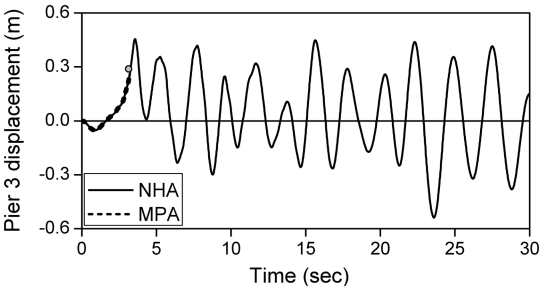

(c) Time history response of pier 3

Fig. 19 Time history response of B42 using MPA (Northridge EQ)

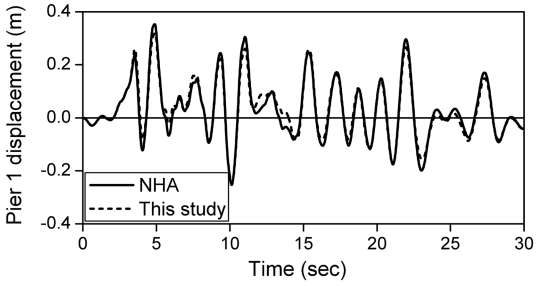

(a) Time history response of pier 1

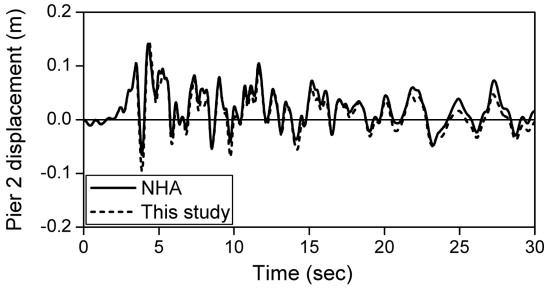

(b) Time history response of pier 2

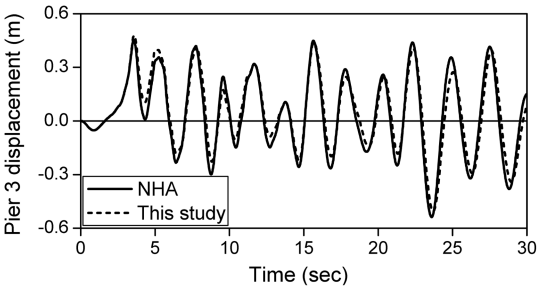

(c) Time history response of pier 3

Fig. 20 Time history response of B42 using IMPA (Northridge EQ)

analyzing a bridge that shows displacement reversal in the capacity curve for a higher mode, but (4), the proposed procedure IMPA can be used effectively to predict the nonlinear seismic response of bridges regardless of any restrictions associated with the bridge configuration.

4.3 Verification of IMPA

To verify the general validity and effectiveness of IMPA and MPA, additional numerical analyses were conducted for symmetric bridge B12 and asymmetric bridge B22 using seven earthquake ground accelerations. When using MPA, the negative work due to displacement reversal in the capacity curve for a higher mode cannot be overcome, even in the case of symmetric bridge B12. Accordingly, for a possible analysis of bridge with MPA, the capacity curves for these modes are

Table 3 Characteristic of the A-D relationship using MPA

Example	Pier	Mode	Stiffness (ω_n^2)	Modal yielding displacement (D_{ny})	Post yield stiffness ratio (α)
B12	1	1st mode	13.254	0.1773	0.323
	2				0.369
	3				0.323
	1	3rd mode	65.629	0.5725	0.485
	2				Assuming perfect
	3				0.485
B22	1	1st mode	15.363	0.1699	0.325
	2				0.420
	3				0.516
	1	2nd mode	45.770	0.1761	0.325
	2				0.414
	3				Assuming perfect
	1	3rd mode	90.225	0.1074	0.391
	2				Assuming perfect
	3				0.851

Table 4 Characteristic of A-D relationship using IMPA

Example	Mode	Stiffness (ω_n^2)	Modal yielding displacement (D_{ny})	Post yield stiffness ratio (α)
B12	1st mode	13.254	0.1562	0.350
	3rd mode	65.629	0.0677	
B22	1st mode	15.363	0.1299	0.407
	2nd mode	45.770	0.0678	
	3rd mode	90.225	0.0429	

assumed to be perfectly plastic after yielding, as these modes can no longer resist a supplemental load. Tables 3 and 4 show the determined characteristics of the capacity curves for the two bridges B12 and B22 when MPA and IMPA, respectively, are used. Based on these capacity curves, SDOF nonlinear time history analyses using Eq. (4) were conducted for each mode considered, and the obtained results were then superposed in order to estimate the maximum displacement ($d_{estimated}$). Finally, the estimated maximum displacements were compared to the maximum displacement ($d_{calculated}$) calculated from the MDOF nonlinear time history analysis using Opensees and the results were used as a reference solution. Figs. 21 and 22 show the relative error-rates determined by $(d_{estimated} - d_{calculated})/d_{calculated}$. As the response of pier 1 is identical with that of pier 3, as shown in Fig. 12, due to the symmetricity in the configuration of bridge B12, the result of pier 3 is abbreviated.

The mean square roots of the square sum of the relative error at each pier were calculated using both the MPA and IMPA methods by Eq. (13), and the obtained error rates are presented in Fig. 23. From this figure, it can be observed that the error rate of the unsymmetrical bridge B22 is greater

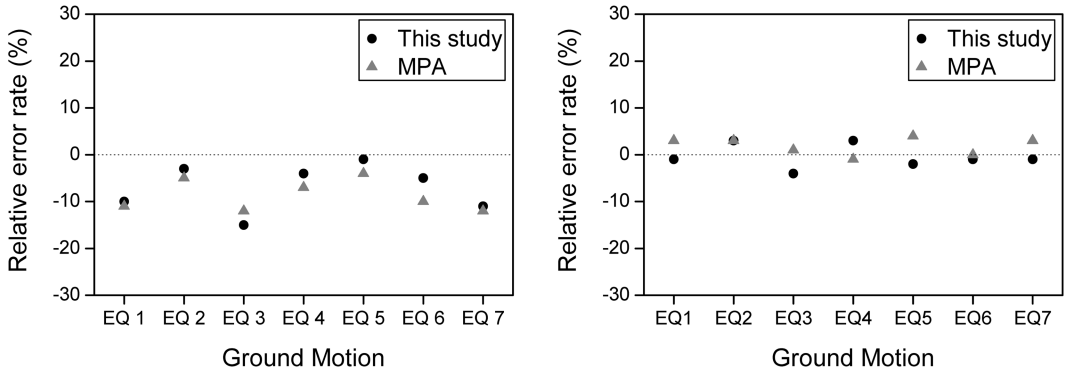

(a) Relative error rate in pier 1 (b) Relative error rate in pier 2

Fig. 21 Relative error rate in B12

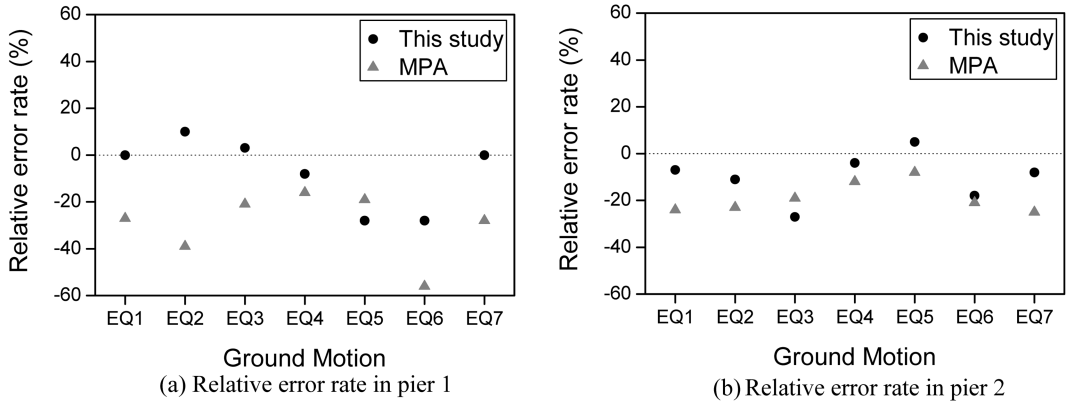

(a) Relative error rate in pier 1 (b) Relative error rate in pier 2

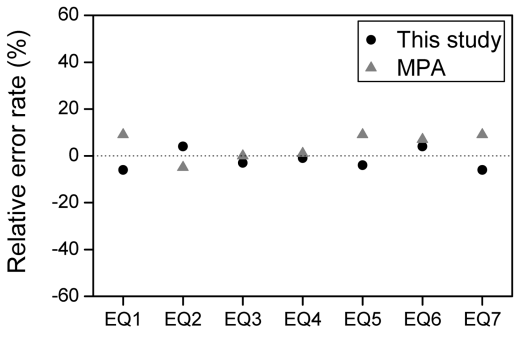

(c) Relative error rate in pier 3

Fig. 22 Relative error rate in B12

than that of the symmetrical bridge B12. Moreover, the error rates of IMPA are nearly identical to those of MPA in the symmetrical bridge B12 but are lower than those of MPA in the unsymmetrical bridge B22, showing that IMPA is more stable and effective. If the assumption of perfect plastic behavior at the yielding stage, introduced in MPA to remove the displacement reversal, is

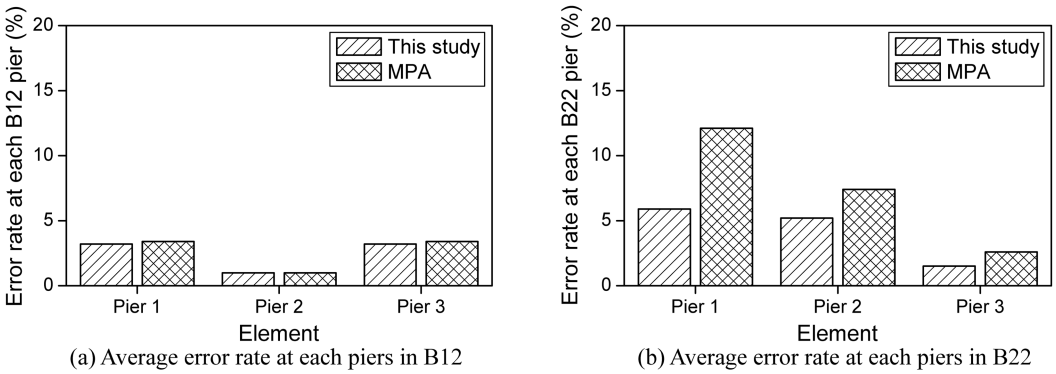

(a) Average error rate at each piers in B12 (b) Average error rate at each piers in B22

Fig. 23 Average error rate for each bridge

maintained, the stability and applicability of IMPA in bridge structures will be enhanced.

$$Error\ Rate(MSRSS) = \frac{1}{N_{EQ}}\sqrt{\sum_{n=1}^{N_{EQ}}\left\{\frac{(Relative\ Error)_n}{(NHA)_n}\right\}^2} \tag{13}$$

5. Estimation of seismic performance through Capacity Spectrum Method (CSM)

In addition to the SDOF nonlinear time history analysis the capacity spectrum method on the basis of the A-D relationship can also be used to evaluate the seismic response of bridge structure. In this case, the use of the capacity spectrum method requires a demand curve as well as a capacity curve. If established demand curves, systematically constructed on the basis of the post-yielding stiffness ratio α ranging from zero to 10% and represented in terms of the A_y–D relationship (Miranda and Bertero 1994, Nassar and Krawinkler 1991) in place of the A–D relationship can be used, only the construction of the capacity curve makes it possible to evaluate the maximum seismic response. However, as shown in Tables 3 and 4, the range of the post-yielding stiffness ratio exceeds 0.1 in typical bridge structures constructed in practice. Accordingly, the demand curves, newly constructed through the SDOF nonlinear time history analysis of the bridge under

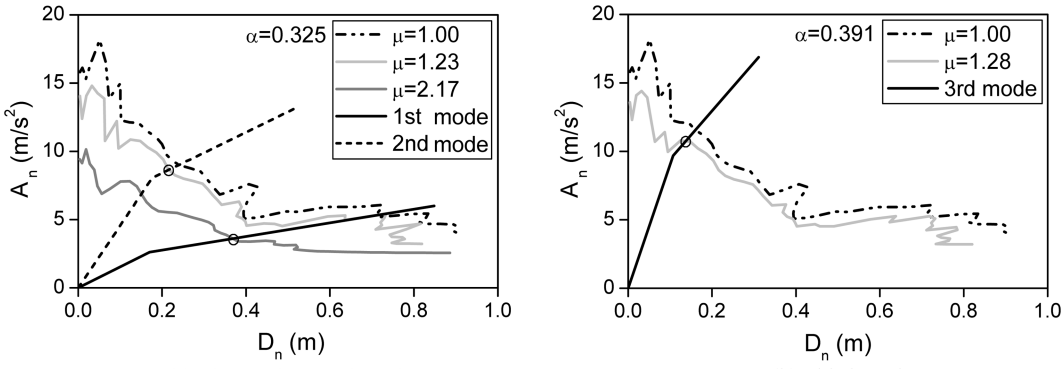

(a) First and second mode (b) Third mode

Fig. 24 Estimation of the performance point for pier 1 of B22 using MPA

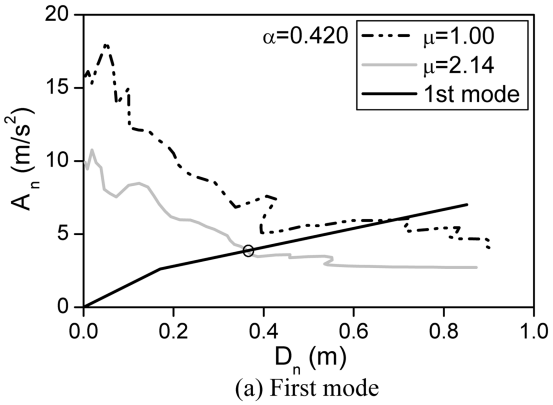

(a) First mode

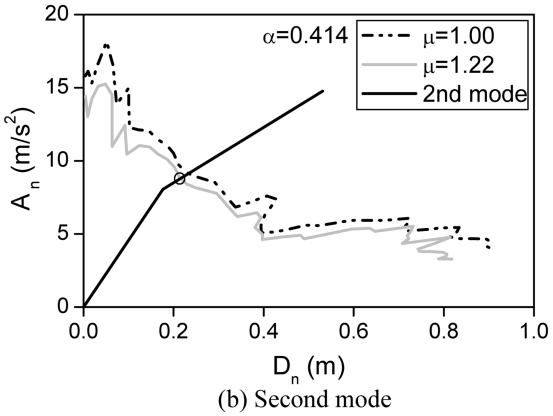

(b) Second mode

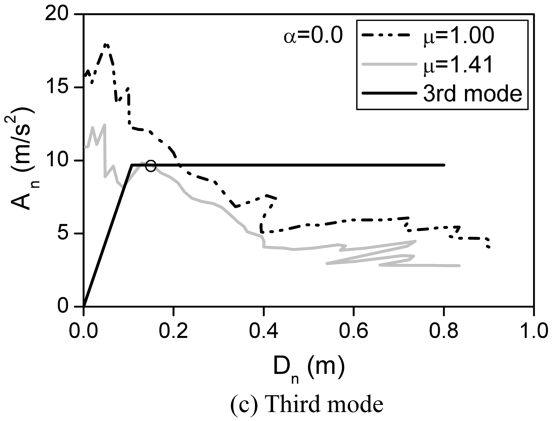

(c) Third mode

Fig. 25 Estimation of the performance point for pier 2 of B22 using MPA

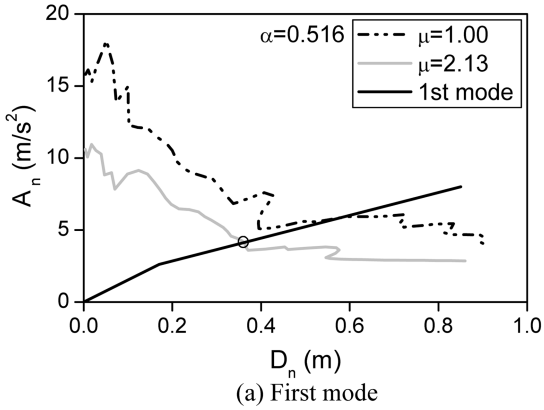

(a) First mode

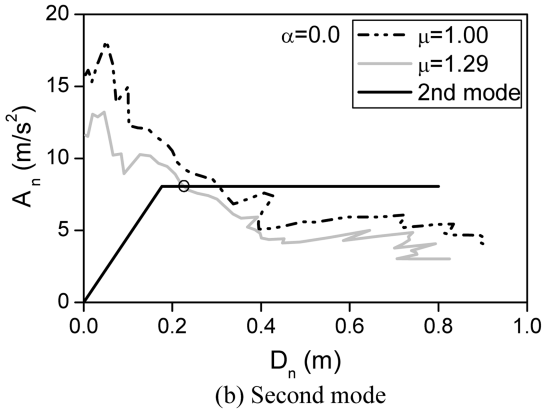

(b) Second mode

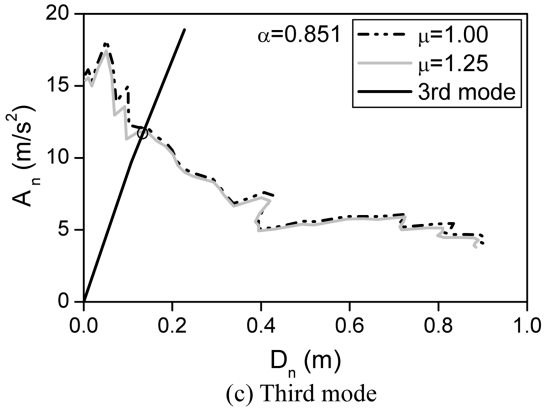

(c) Third mode

Fig. 26 Estimation of the performance point for pier 3 of B22 using MPA

consideration here, are used in this paper.

Figs. 24 to 26 show the capacity spectrum method (CSM) for determining the maximum displacement of B22 using MPA. The maximum modal displacements D_{n0}, in which the demand curve and the capacity curve cross each other while satisfying the consistent ductility, are marked with circles. These figures explain is the difficulty with which MPA calculates the maximum modal displacement, as the inelastic demand curves must be reconstructed when the stiffness ratio α changes.

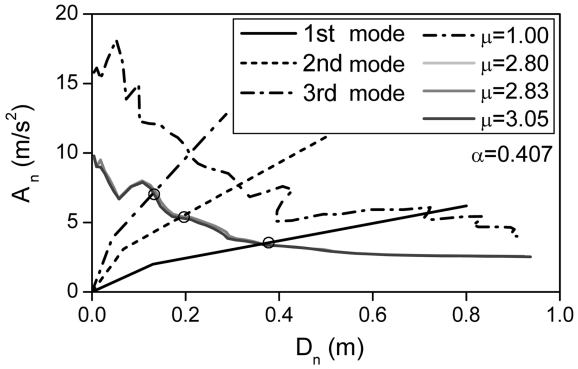

Fig. 27 Estimation of the performance point of B22 using IMPA

Compared to MPA, however, the IMPA procedure is relatively simple because this method requires the construction of only one set of demand curves corresponding to each vibration mode as a result of the constant stiffness ratio. As an example, bridge B22 has a constant stiffness ratio of 0.407 (see Fig. 27). Specifically, unlike MPA, which requires nine sets of demand curves due to the different ratio, IMPA requires only three sets of demand curves in the case of bridge B22. After determination of the maximum displacement D_{n0} in each example in Figs. 24 to 27, the modal maximum displacement at pier r can be calculated by $u_{rno} = \Gamma_n \phi_{rn} D_{n0}$ and the maximum displacement at pier r ($(u_{pier,r})_{\max}$ in Table 5.) can then be obtained through the modal combination rule by SRSS. From Table 5 which shows the obtained maximum displacements at each pier, it can be observed that both the MPA and IMPA methods can effectively estimate the maximum displacement of B22, although IMPA shows a slight difference at pier 1 compared to the reference value by NHA. This difference, however, appears to be negligibly small. Nonetheless, as an approximate method, IMPA can be used with greater effectiveness compared to MPA in bridge structures as it requires only one pushover analysis to determine the capacity curve and the construction of one set of inelastic demand curves corresponding to the specific constant post-yield stiffness ratio. Furthermore, the proposed method is more stable and does not experience displacement reversal in the capacity curve for a higher mode.

Table 5 Estimated maximum displacements of B22 through CSM (unit: m)

Pier	mode	NHA	MPA		IMPA	
		$(U_{pier_r})_{\max}$	D_{n0}	$(U_{pier_r})_{\max}$	D_{n0}	$(U_{pier_r})_{\max}$
1	1st mode	0.114	0.369	0.112	0.364	0.105
	2nd mode		0.216		0.192	
	3rd mode		0.137		0.131	
2	1st mode	0.316	0.363	0.311	0.364	0.307
	2nd mode		0.215		0.192	
	3rd mode		0.151		0.131	
3	1st mode	0.445	0.361	0.444	0.364	0.445
	2nd mode		0.226		0.192	
	3rd mode		0.135		0.131	

6. Conclusions

This paper focuses on the introduction of improved modal pushover analysis (IMPA) that can estimate the seismic performance of a multi-span bridge structure. Through correlation studies between the proposed method (IMPA) and the established methods of ESDOF, PSDOF and MPA for typical bridges, the following conclusions were obtained: (1) ESDOF has limitations when estimating the seismic performance of a bridge with a low-stiffness super-structure, and both PSDOF and ESDOF may increase incidence of numerical error when predicting the structural response of an unsymmetrical bridge. On the other hand, the conventional MPA occasionally produces displacement reversal in the modal pushover curve for a higher mode, which makes a seismic analysis of bridge impossible; (2) unlike the previously established methods of ESDOF, PSDOF and MPA, the proposed method of IMPA can be used effectively to estimate the seismic performance of all bridge structures regardless of the bridge configuration. Furthermore, an introduction of a constant post-yield stiffness ratio together with an approximated elastic deformation makes it possible to remove the coupling effect between each vibration mode and clarifies that the proposed method is based on more robust theory; (3) the proposed method is simpler than most established methods, as it requires only one pushover analysis and one set of demand curves despite the fact that it considers all of the vibration modes; finally, (4) the proposed method can be used effectively to estimate the seismic performance of multi-span continuous bridge structures through a SDOF time history analysis and/or the capacity spectrum method. Nevertheless, additional parametric studies and/or more improvement in the solution procedure may be required before IMPA is applicable to bridges with relatively large nonsymmetrical configurations.

Acknowledgements

This research was supported by a grant (07High Tech A01) from High tech Urban Development Program funded by Ministry of Land, Transportation and Maritime Affairs of Korean government and from the Smart Infra-Structure Technology Center funded by the Korea Science and Engineering Foundation.

References

Bozorgnia, Y. and Bertero, V.V. (2004), *Earthquake Engineering from Engineering Seismology to Performance-based Engineering*, CRC Press, Boca Raton at Florida.

Chopra, A.K. and Goel, R.K. (1999), *Capacity-demand-diagram Methods for Estimating Seismic Deformation of Inelastic Structures: SDF Systems*, Report No. PEER-1999/02, Pacific Earthquake Research Center, University of California at Berkeley.

Chopra, A.K. (2001), *Dynamics of Structures: Theory and Application to Earthquake Engineering*, Prentice-Hall: Englewood Cliffs, NJ.

Chopra, A.K. and Goel, R.K. (2002), "A modal pushover analysis procedure for estimating seismic demands for buildings", *Earthq. Eng. Struct. Dyn.*, **31**, 561-582.

Chopra, A.K. and Goel, R.K. (2004), "A modal pushover analysis procedure to estimate seismic demands for unsymmetric-plan buildings", *Earthq. Eng. Struct. Dyn.*, **33**, 903-927.

Elnashai, A.S. (2001), "Advanced inelastic static (pushover) analysis for earthquake applications", *Struct. Eng.*

Mech., **12**, 51-69.
Freeman, S.A. (1998), *Development and Use of Capacity Spectrum Method*, Proceedings of 6th U.S. National Conference on Earthquake Engineering. Seattle, EERI, Oakland, California.
Krawinkler, H. and Seneviratna, G.D.P.K. (1998), "Pros and cons of a pushover analysis of seismic performance evaluation", *Eng. Struct.,* **20**(4-6), 452-464.
Lakshmana, N., Gopalakrishnan, N., Rama Rao, G.V. and Sathish Kumar, K. (2009), "Dynamic stiffness based computation of response for framed machine foundation", *Geomech. Eng.,* **1**(2), 121-142.
Miranda, E. and Bertero, V.V. (1994), "Evaluation of strength reduction factors for earthquake-resistant design", *Earthq. Spect.,* **10**, 357-379.
Nassar, A.A. and Krawinkler, H. (1991), *Seismic Demands for SDOF and MDOF Systems*, John A. Blume Earthquake Engineering Center, Report No.95, Stanford University, CA.
Nickell, R.E. (1976), "Nonlinear dynamics by mode superposition", *Comput. Meth. Appl. Mech. Eng.,* **7**, 107-129.
Song, J.G. (2004), "Evaluation of inelastic seismic response of multi-degree-of freedom bridge structures using capacity spectrum method", *J. Korean Soc. Civil Eng.,* **4**(3A), 541-550.
Takeda, T., Sozen, M.A. and Nielsen, N.N. (1970), "Reinforced concrete response to simulated earthquake", *J. Struct. Div.*, **96**(ST-12), 2557-2573.
Usanmi, T., Lu, Z., Ge, H. and Kono, T. (2004), "Seismic performance evaluation of steel arch bridges against major earthquakes. Part 1: Dynamic analysis approach", *Earthq. Eng. Struct. Dyn.*, **33**, 1337-1354.
Usanmi, T., Lu, Z., Ge, H. and Kono, T. (2004), "Seismic performance evaluation of steel arch bridges against major earthquakes. Part 2: Simplified verification procedure", *Earthq. Eng. Struct. Dyn.*, **33**, 1355-1372.
Zheng, Y., Usanmi, T. and Ge, H. (2003), "Seismic response prediction of multi-span bridges through pushover analysis", *Earthq. Eng. Struct. Dyn.*, **32**, 1259-1274.